

Variation of the ultraviolet extinction law across the Taurus-Auriga star forming complex. A GALEX based study.

Ana I. Gómez de Castro¹, Javier López-Santiago¹, Fátima López-Martínez¹,
Néstor Sánchez¹, Elisa de Castro² and Manuel Cornide²

¹*AEGORA Research Group, Universidad Complutense de Madrid, Plaza de Ciencias 3, 28040 Madrid, Spain*

²*Fac. de CC. Físicas, Universidad Complutense de Madrid, Plaza de Ciencias 1, 28040 Madrid, Spain*

Submission, October 15th, 2013

ABSTRACT

The Taurus-Auriga molecular complex (TMC) is the main laboratory for the study of low mass star formation. The density and properties of interstellar dust are expected to vary across the TMC. These variations trace important processes such as dust nucleation or the magnetic field coupling with the cloud. In this article, we show how the combination of near ultraviolet (NUV) and infrared (IR) photometry can be used to derive the strength of the 2175 Å bump and thus any enhancement in the abundance of small dust grains and PAHs in the dust grains size distribution. This technique is applied to the envelope of the TMC, mapped by the GALEX All Sky Survey (AIS). UV and IR **photometric** data have been retrieved from the GALEX-AIS and the 2MASS catalogues. NUV and K-band star counts have been used to identify the areas in the cloud envelope where the 2175 Å bump is weaker than in the diffuse ISM namely, the low column density extensions of L1495, L1498 and L1524 in Taurus, L1545, L1548, L1519, L1513 in Auriga and L1482-83 in the California region. This finding agrees with previous results on dust evolution derived from Spitzer data and suggests that dust grains begin to decouple from the environmental galactic magnetic field already in the envelope.

Key words:

ISM: clouds - dust, extinction

1 INTRODUCTION

Molecular clouds are not isolated entities in the galactic interstellar medium. They are produced at locations where diffuse gas in the Galaxy is gathered due to the action of galactic stresses basically, spiral waves exciting Parker-Jeans instability modes (Elmegreen 1990, Franco et al. 2002) though eventually accretion from the intergalactic medium cannot be neglected (Mirabel 1982, Wang et al. 2004).

Molecular clouds form in large structures or *molecular complexes* in specific areas of the Galaxy. The Taurus-Auriga Molecular Complex (TMC) covers about $20^\circ \times 20^\circ$ in the sky. The TMC is the prototype of filamentary molecular complex where star formation proceeds less efficiently than in massive clusters, such as the L1630 cloud in the Orion molecular complex (Lada 19922). The large filamentary structure of the TMC is reminiscent of the galactic open clusters distribution.

Molecular clouds are submitted to the ionising radia-

tion field of the Galaxy that produces photo evaporative flows on the surface. The hardness of the ultraviolet (UV) radiation field around the TMC can be readily inferred from the SPEAR/FIMS imaging spectrograph observations. The cloud core and the halo region are clearly identified (**Lee et al. 2006**). The scattered far UV (1370Å – 1670Å) radiation is seen in, and beyond, the halo region (where $A_v < 1.5$ mag) as plumes in photo-evaporative flows, on the scale of the SPEAR/FIMS resolution: 5-10 arcmin or 0.2-0.4 pc. Mapping the diffuse emission and the extinction variations at those optical depths provides important information on the physics of the cloud boundary that, contrary to the cloud interior, is not dominated by the gravitational field but by more subtle stresses. Moreover, there is recent evidence of additional heating sources in the edge of the TMC, since the diffuse galactic UV radiation field cannot solely account for the degree of excitation of the molecular Hydrogen (Goldsmith et al. 2010).

Cloud haloes may provide important clues on the transmission/reflection of long wavelength modes of the galactic magnetic field, as those hypothesised by Gómez de Castro & Pudritz (1992, hereafter GdCP92) to describe the global properties of the Taurus star-forming region. The geometry of the magnetic field in Taurus has been traced by optical and infrared polarisation measurements (Vrba et al. 1976, Moneti et al. 1984, Heyer et al. 1987, Goodman et al. 1990, Chapman et al. 2011). The observations indicate that the field is well ordered on the scale of the whole cloud, but that it also contains a significant disordered component on the smaller scales (Goodman et al. 1990). Zeeman measurements of the field strength in molecular clouds indicate that magnetic and gravitational energy density are comparable. Thus, magnetic fields must play a fundamental role in the dynamics of the cloud and the formation of structures such as the ubiquitous cores and filaments. The orientation of the magnetic field with respect to the dense filament substructure can vary from perpendicular to parallel alignments depending upon the filament (Vrba et al. 1976, Heyer et al. 1987, Goodman et al. 1990). A recent evaluation of the field relevance in the gas flow suggests that magnetic fields control the mass flow in the TMC diffuse envelope. Heyer & Brunt (2012) studied the alignment of the velocity anisotropy with the magnetic field over varying physical conditions and environments to conclude that the velocity anisotropy is aligned with the local, projected mean magnetic field direction in low surface brightness ^{12}CO emission areas, corresponding to regions of low visual extinction and presumably, low gas volume density. This would be consistent with the presence of a large scale Alfvén wave channelling the dynamics of the TMC, as suggested by GdCP92.

The coupling between the clouds and the ambient field relies on the dust grains ionisation and mass spectrum. Dust grains contain most of the mass of the charged particle component in the molecular clouds interior. For typical clouds, the cut-off wavelength for the coupling with the ambient field decreases from 1 pc to 0.1 pc when dust grains are considered (Nakano, 1998). Also, the size of the dust grains is relevant for the resonance frequencies to Alfvén waves propagation and the neutral-charge particles coupling (Pilipp et al. 1987). The near ultraviolet bump (the 2175 Å bump) is the most sensitive feature to the presence of small dust grains (see i.e. Draine 2003) and hence, to plasma field coupling. Therefore, though the use of spectral tracers able to penetrate the dusty environment (infrared, X-ray, radio-wavelengths) is useful to study the gravitational collapse and the cloud fragmentation, important pieces of information leading to cloud formation and support are best accessed through UV observations.

The GALactic Evolution eXplorer (GALEX) has surveyed the envelope of the TMC complex permitting a **study of** the dust spatial distribution with a sensitivity significantly higher than the conventional means (molecular or infrared mapping). Moreover, as the TMC is a well studied region, comprehensive mapping in various molecular probes such as CO (Ungerechts & Thaddeus 1987, Heyer et al. 1987, Goldsmith et al. 2008, Davis et al. 2010), NH_3 (Benson & Myers, 1983, Gaida et al. 1984, Olano et al. 1988, Ladd et al. 1994) as well as in the infrared range (Froeblich et al. 2007, hereafter F07, Lombardi et al. 2010, hereafter LLA10) is available allowing to study the relation between gas and

dust density in various bands. For instance, the comparison between the relative extinctions in the GALEX NUV band, centred at the 2175 Å bump, and in the K band from the 2MASS survey (LLA10) permits to evaluate variations in the average dust grains size over the TMC in a very efficient manner. Evidence of dust grain growth in dense molecular gas filaments compared with the diffuse interstellar medium (ISM) have been recently, reported from infrared studies (see *e.g.* Ysard et al 2013 study for the L1506 filament in Taurus or Flagey et al. 2009 for a Spitzer based study).

The UV bump is, by far, the strongest spectral feature in the extinction curve but its source remains uncertain (see *e.g.* the review by Draine 2003). Though small graphite grains were proposed initially as the main source of the bump, the baseline today are polycyclic aromatic hydrocarbon (PAH) molecules (Weintgarner & Draine, 2001), that share with a graphite sheet, a similar structure in terms of the distribution of the carbon atoms. PAHs are required to reproduce the observed infrared emission (Leger & Puget, 1984) and they somewhat represent the extension of the dust grain size distribution into the molecular domain.

In this article, we derive a method to determine the strength of the 2175 Å bump from a combination of extinction measurements in the GALEX near UV (NUV) band and the 2MASS K infrared band (see Sect. 2). In Section 3, we describe the GALEX All Sky Survey of the TMC, the quality and main characteristics of the data. In Section 4, we describe the method used to measure the extinction in the NUV band in the TMC and the results are analysed in Section 5. It is shown that the strength 2175 Å bump decreases with respect to the average ISM values in the filaments gathering areas, namely, the low column density extensions of L1495, L1498 and L1524 in Taurus, L1545, L1548, L1519, L1513 in Auriga and L1482-83 in the California region. These finding agrees with previous results on dust evolution derived from Spitzer data. This indicates that within the halo of the molecular clouds, the dust grains are already rather large, affecting the coupling between the dust and the environmental magnetic field. A brief summary is provided at the end of the article.

2 A METHOD TO MEASURE THE STRENGTH OF THE 2175 Å BUMP FROM A_{NUV} AND A_K

The extinction curve provides important clues about the properties of dust in space and the grains size distribution (see, for instance the review by Draine 2003 and references therein). The shape of the extinction curve is often modelled using to polynomial fits that extend from the far UV to the infrared using as free parameter $R_V = A_V/E(B - V)$. In this work, we use the widespread extinction model derived by Fitzpatrick & Massa 2007 (hereafter FM07).

The curve is well behaved from the 3 μm to 0.3 μm ; it allows a simple parametrisation in the infrared that extends smoothly into the optical range so,

$$\frac{A_K}{A_V} = 1 + \frac{1}{R} k(K - V) \quad (1)$$

with $k(K - V) = (-0.83 + 0.63R)\lambda^{-1.84} - R$ and $\lambda = 2.2 \mu\text{m}$ for the average extinction law according to FM07. Hence,

$$\frac{A_K}{A_V} = 1 + \frac{1}{R}(-0.19 - 0.85R) \quad (2)$$

This smooth trend is broken in the UV range by the presence of the UV bump; five coefficients are required for the mathematical representation of the extinction law in the UV (see Eq. 3), two of them to fit the UV bump to a Lorentzian function of $(1/\lambda)$. Following FM07, the extinction law in the NUV band is parametrised as,

$$k(\lambda - V) = E(\lambda - V)/E(B - V) = \quad (3)$$

$$c_1 + c_2x + c_3D(x, x_0, \gamma)$$

with $x = 1/\lambda(\mu m)$ and,

$$D(x, x_0, \gamma) = \frac{x^2}{(x^2 - x_0^2)^2 + x^2\gamma^2} \quad (4)$$

Parameters c_1, c_2, c_3, x_0 and γ are constants that depend on the specific line of sight. The area of the bump is given by $A_{\text{bump}} = \pi c_3/(2\gamma)$ and its maximum intensity by $I_{\text{bump}} = c_3/\gamma^2$.

The width of the bump varies considerably from line of sight (LoS) to LoS with an average value of $0.993\mu m^{-1}$ but its central wavelength remains stable (Fitzpatrick & Massa, 1986). Absorption by small graphite particles was first hypothesised, as the main source of this strong absorption however, variations in the graphite grain shape and size should produce variations both in γ and x_0 (Draine & Malhotra 1993). Since the molecular structure of PAHs molecules is very similar to a portion of a graphite sheet, PAHs are a natural extension to the graphite hypothesis and are nowadays considered the main source of the bump (see Draine 2003 review for more details).

By definition,

$$\frac{A_{NUV}}{A_V} = 1 + \frac{1}{R}k(NUV - V) \quad (5)$$

where $k(NUV - V)$ is weighted over the GALEX NUV band. Hence,

$$k(NUV - V) = \quad (6)$$

$$\int_{x_1}^{x_2} g_{NUV}(x)(c_1 + c_2x + c_3D(x, x_0, \gamma))dx$$

$$= c_1 <g_{NUV}> + c_2 <xg_{NUV}> + c_3 <g_{NUV}(x)D(x, x_0, \gamma)>$$

with $g_{NUV}(x)$ the normalised transmittance function of the GALEX NUV channel¹, $x_1 = 1680 \text{ \AA}$ and $x_2 = 3000 \text{ \AA}$. Thus, by definition,

$$<g_{NUV}> = \int_{x_1}^{x_2} g_{NUV}(x)dx = 1 \quad (7)$$

and,

$$<xg_{NUV}> = \int_{x_1}^{x_2} xg_{NUV}(x)dx = 4.49 \quad (8)$$

The third term in **Eq. 6** depends on γ since **it influences** $D(x, x_0, \gamma)$. We have evaluated this integral for the various γ values in FM07; they correspond to different LoS and extinction laws in the Galaxy. We have found that the integral can be fitted to a linear function of γ such that,

Table 1. The standard extinction law in the GALEX NUV band

LoS	R ^(a)	$\frac{A_{NUV}}{A_V}$	$\frac{A_K}{A_V}$	$R(NUV - K)^{(b)}$	$\frac{A_{NUV}}{A_K}$
HD698	3.94	2.56	0.09829	9.7	26.05
HD3191	2.81	2.923	0.07843	7.993	37.26
BD+57 245	2.97	2.828	0.08216	8.156	34.42
BD+57 252	2.97	2.889	0.08216	8.335	35.16
NGC457 P34	2.94	2.806	0.08149	8.011	34.44
NGC457 P13	3.11	2.588	0.08511	7.784	30.41
NGC457 P9	2.76	3.089	0.07718	8.314	40.03
ISM average	3.001	2.735	0.08284	7.958	33.01

$$^{(a)} \quad R = A_V/E(B - V)$$

$$^{(b)} \quad R(NUV - K) = (A_{NUV} - A_K)/E(B - V)$$

$$<g_{NUV}(x)D(x, x_0, \gamma)> = \quad (9)$$

$$-(0.82 \pm 0.02)\gamma + (1.38 \pm 0.02)$$

with rms=0.003. This tight correlation was expected given the functional form of $D(x, x_0, \gamma)$ in the GALEX band and the strength of the 2175 Å feature. Since the area of the 2175 Å bump also depends on γ , $A_{\text{bump}} = \pi c_3/2\gamma$, then,

$$<g_{NUV}(x)D(x, x_0, \gamma)> = -1.29A_{\text{bump}}^{-1}c_3^2 + 1.38 \quad (10)$$

and therefore,

$$\frac{A_{NUV}}{A_K} = \frac{R + c_1 + 4.49c_2 + c_3(-1.29A_{\text{bump}}^{-1}c_3^2 + 1.38)}{0.15R - 0.19} \quad (11)$$

FM07 made a detailed evaluation of the extinction law parameters for several LoSs (see Table 4 in their article) and using them, we have computed the A_{NUV}/A_V , A_K/A_V and A_{NUV}/A_K values for these specific LoSs; also, we have computed them for the average ISM coefficients² as derived by FM07 (see Table 1).

In general, our $R(NUV-K)$ is slightly larger than the values computed by Yuan et al. (2013), $R(NUV-K) = 6.75$, as well as their evaluation from the FM07 extinction law $R(NUV - K) = 6.31$.

A_{NUV}/A_K and A_{bump} have been evaluated for all the LoS in FM07 (see Table 1) and plotted in Fig. 1. Notice that A_{NUV}/A_K and A_{bump} values are well correlated unless for HD 3191, which seems to be a peculiar³. For this reason, it has been excluded, **and the resulting fit in Fig. 1 is:**

$$A_{\text{bump}} = (0.106 \pm 0.008)\frac{A_{NUV}}{A_K} + (2.0 \pm 0.3) \quad (12)$$

This result is not a surprising; it just points out that the ISM extinction law admits a rather simple parametrisation from the near infrared to the near ultraviolet unless for the strength of the bump. Therefore, for the dust grain size distributions observed in the ISM, the main deviations from this trend are caused by the UV bump.

Likewise, the strength of the bump can be evaluated as a linear function of the NUV to K band extinction for the ISM. Note that this *semi-empirical relation* has been derived using the LoSs in FM07 that sample a broad range

² Parameters values for the average galactic extinction curve are: $x_0 = 4.592 \mu m^{-1}$, $\gamma = 0.922 \mu m^{-1}$, $c_1 = -0.175$, $c_2 = 0.807$ and $c_3 = 2.991$.

³ HD 3191 also affects significantly the average ISM law, as parametrized by FM07

¹ <http://galexgi.gsfc.nasa.gov/docs/galex/Documents/>

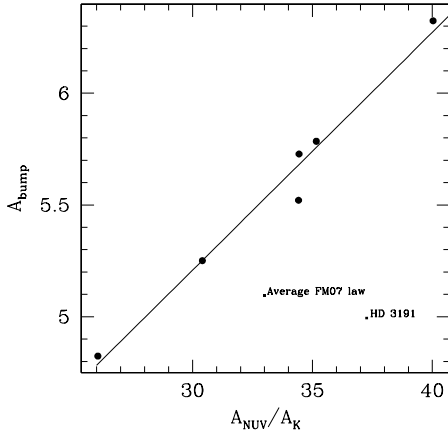


Figure 1. Relation between the area of the 2175 Å bump and the relative NUV versus K extinction for the FM07 extinction law.

of extinction laws (*i.e.*, R-values and bump strengths) and it is independent of the physical origin of the bump be it PAHs, small graphite grains or any other possible source (*e.g.* fullerens, see Wada et al. 1999).

In principle, similar expressions could be derived for other bands however, the availability of the near infrared extinction map of the TMC (LLA10) makes the A_{NUV}/A_K rate, well suited for our purpose. Note that emission from average warm dust grains dominate the K-band while absorption by PAHs or alike dominates the NUV band.

Mid-infrared images have also been used to test dust evolution by comparing the emission from PAHs and very small grains with the radiation from large dust grains (see *i.e.* Flagey et al. 2010). However, the NUV range is ideally suited for this purpose given its high sensitivity to small particles; the estimated oscillator strength per nucleon is $n_X f_X/n_H \simeq 9.3 \times 10^{-6}$ for the 2175 Å bump (Draine, 1989).

For completeness, we also note that,

$$A_{NUV} - A_K = E(B - V)(0.19 + c_1 + 4.49c_2 - 1.29A_{\text{bump}}^{-1}c_3^3 + 1.38c_3 + 0.85R) \quad (13)$$

and thus, $(A_{NUV} - A_K)/E(B - V)$ can be parametrised in terms of the strength of the bump and, as above, a simple scaling can be made in terms of the extinction law for various LoS,

$$A_{\text{bump}} = (2.4 \pm 0.5) \frac{A_{NUV} - A_K}{E(B - V)} - (0.9 \pm 1.5) \quad (14)$$

though the fit is significantly less accurate (see Fig. 2).

3 THE GALEX SURVEY OF THE TMC

The baseline of the GALEX All Sky Survey was completed in 2007. GALEX AIS covers 26,000 deg² ($\sim 63\%$ of the Sky) and provides broadband imaging in two UV bands.

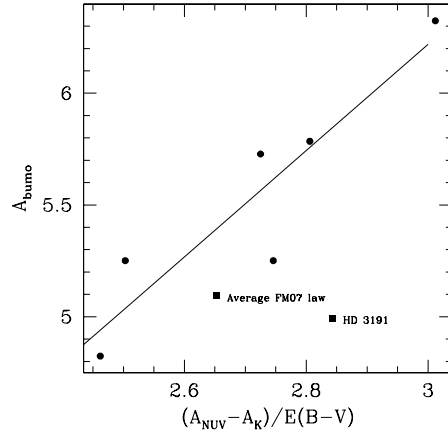


Figure 2. Relation between the area of the 2175 Å bump and the $(A_{NUV} - A_K)/E(B - V)$ for the FM07 extinction law.

GALEX obtained 197 images on the Taurus molecular cloud with a total coverage of ~ 200 deg² (see Fig. 3); note that the GALEX field of view is circular with radius 0.6°. The survey avoids the central region of the TMC where TMC-1 is located, though some pointings are made around TMC-2. Some molecular cores like L1495, L1498, L1544, L1515, L1548 and L1552 are partially covered in the survey.

The GALEX mission provides as output products for each tile (or image in the AIS survey) several files containing the pipeline processed images in the FUV and NUV bands, the intermediate calibration files and the catalogue of sources identified in each pointing; the sources in the catalogue are identified with the SExtractor procedure (Morrissey et al. 2007) and their FUV and NUV magnitudes are provided. Typically, the number of sources in the catalogue outnumbers by a factor of 2-3, the number of sources that can be identified as such from a simple inspection of the images. The detection procedure clearly suffers from overestimation of actual sources. The number of spurious detections is very large.

As the TMC is close to the galactic plane, a cross-identification with galactic sources from the Fourth USNO CCD Astrograph Catalog - U.S. Naval Observatory (UCAC4; Zacharias et al. 2013) and the 2MASS surveys (Strutskie et al. 2006) has been carried out. Typically, for each of our GALEX fields, there are a factor of 3 more sources in the 2MASS survey and a factor of 10 in the UCAC4 survey; thus, they outnumber by far the UV sources identified by the GALEX pipeline and can be used to check the reliability of the GALEX identification. To complete the cross-identification of our sample with sources at different wavelengths, we have also cross-correlated our list with the WISE all-sky catalogue (Cutri et al. 2012) using the same criteria than for the other two databases.

Magnitude completeness limits for 2MASS are 15.8, 15.1 and 14.3 mag in J, H and K_s bands, respectively. These

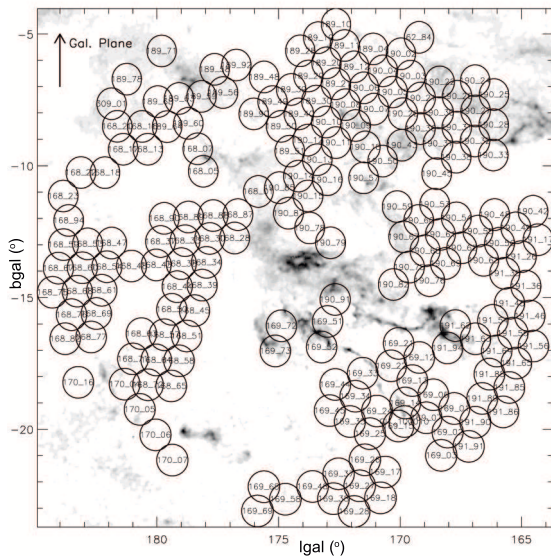


Figure 3. Fields observed by GALEX (AIS GR5) towards the Taurus Molecular Complex (open circles) are overlaid on the map of hydrogen column density (N_H) produced by LLA10 from 2MASS star counts.

limits are well above the magnitude of M-type stars at the distance of the Taurus-Auriga molecular complex. J magnitude for a 4 Myr old M5 star is ~ 5.5 (e.g. Siess et al. 2000). At a distance of 140 pc, the magnitude of such star $J \sim 11.5$ mag. Even in the case of notably ISM extinction $A_J = 4$ mag, the star would be detected by 2MASS at the distance of the molecular cloud. Similarly, UCAC4 is complete from the brightest stars to about $R = 16$ mag. This means that UCAC4 is complete for mid-M stars at the distance of the Taurus cloud for extinctions $A_V < 2$ mag. As we do not expect large extinctions for our stars, because they were selected from the UV, we can conclude that we are complete for members of the star-forming region for the entire luminosity function, from the more massive to the less massive stars. Completeness limit for a typical 100s exposure time GALEX/AIS image in NUV and FUV is ~ 20 mag in both cases (Bianchi et al. 2013).

Bona fide GALEX sources have been identified by having a 2MASS counterpart within a search radius of 3 arcsec. This search radius was carefully selected after a precise study of the shift between 2MASS and GALEX sources in the TMC (see Gómez de Castro et al 2011 for details). After the cross-correlation, we kept a total of 163,313 UV sources as reliable detections. All them have been detected in the NUV band but only 10% of the sources have a FUV counterpart. Since this research is based on stellar statistics, we worked with the sample of confirmed NUV sources (163,313 sources). Only 31 TTs and 63 candidates to TTs are found in the area covered by this survey (Gómez de Castro et al. 2015) thus, their impact in the overall statistics is minimum.

In Fig. 4, the surface density of stars towards the TMC is plotted; the location of the main molecular cores as well as the brightest UV sources in the field (from Lee et al. 2006) are marked. The NUV surface density of stars is overlaid on the large scale extinction map of the area obtained by

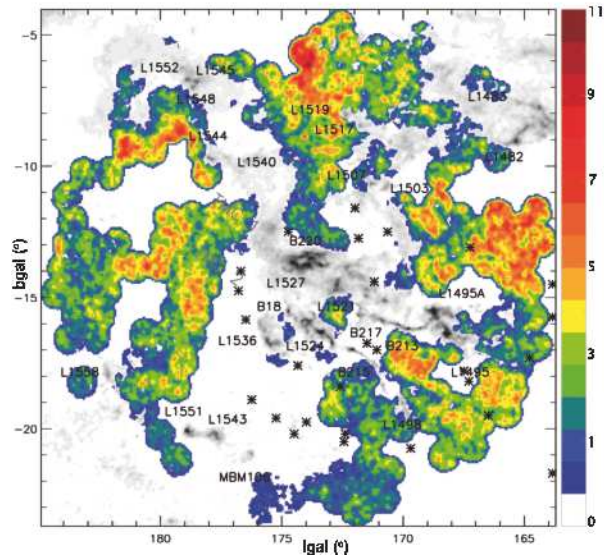


Figure 4. Density of NUV GALEX sources in the TMC. The densities are colour coded in stars per 3 arcmin² (see lateral bar). The 2MASS extinction map (LLA10) is overlaid for reference. The location of the main molecular cores and the main UV sources in the field (asterisks) are marked.

Lombardi et al (2010) from the 2MASS survey of the TMC. A comparison between both maps (see also Fig. 4 in LLA10), points out that most of the area surveyed by GALEX has $A_K \leq 0.2$ mag that roughly corresponds⁴ to $A_V \leq 2.2$ mag (or $N_H \leq 4 \times 10^{21}$ atoms cm⁻²). The density of stars drops to zero at higher gas columns. For instance, the extension of some well known filaments, such as L1495 or L1498, shows in the stellar density map because the density of stars drops to 0. Also, some diffuse structures are noticeable. For instance, at $b_{gal} = -13^\circ$, the stellar density varies from 5-6 stars per 3 arcmin² at $l_{gal} = 165^\circ$ (westwards of the TMC) to 2-3 stars per 3 arcmin² at $l_{gal} = 180^\circ$; this feature passed unattended in previous CO maps of the area.

4 METHODS

4.1 The Wolf method

The Wolf method is designed to measure extinction using as reference for the stellar luminosity function a nearby stellar field, assumed to be unextincted. The luminosity function is defined in terms of the cumulative star counts distribution per apparent magnitude bin, in the fiducial field (Wolf 1923: see also Gorbikov & Brosch, 2011 for a recent application of the method to study the extinction law towards the north celestial cap). The method is based on the fact that all the stars behind the same absorbing cloud are extinguished by the same amount, A_λ . As a result, the cumulative star counts distribution as a function of the apparent magnitude, $N(m(\lambda))$, is homogeneously shifted to lower apparent

⁴ The average ISM extinction law, as described in Sect. 2, has been used for this scaling.

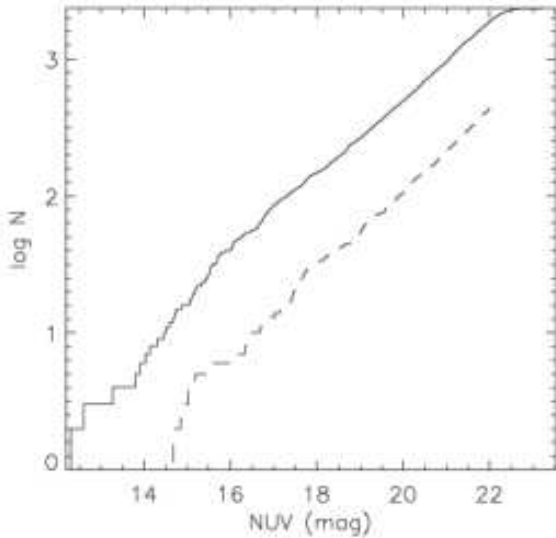


Figure 5. Determination of the extinction using the Wolf method for tile AIS190_sg27. The plot illustrates the cumulative counts distribution in AIS190_sg27 (solid line) compared with AIS189_28, the reference tile (dashed).

magnitudes in any dusty area. The shift of the cumulative counts distribution is a direct measure of the relative extinction between the fiducial field and any given field. The process is illustrated in Fig. 5 for tile AIS190_sg57. A control tile, tile AIS189_28, has been used for calibration purposes since extinction is not apparent neither in the UV data (see Fig. 3) nor in the infrared data (see LLA10). The NUV cumulative distribution in AIS190_sg297 is clearly shifted with respect to the reference field pointing out a NUV extinction of $A_{NUV} = 2.8$ mag.

Following this procedure both A_{NUV} and A_K values have been computed however, the A_{NUV}/A_K ratios obtained are unusually small and inconsistent with the interstellar extinction law (*e.g.* FM07). These small ratios are obtained because the GALEX AIS fields contain areas with and without dust clouds; this geometric dilution together with the clumpiness of the ISM produces a weighted average of the A_{NUV}/A_K value over the GALEX AIS field of view (see Appendix A for more details). Therefore, it is critical to work with spatial resolutions that adapt well to the characteristic scales of the ISM structures to be studied such as filaments, globules etc, typically about 0.1-0.4 pc.

Unfortunately, the Wolf method requires a good statistics to sample properly the luminosity function forcing the resolution element to be much larger than 0.1-0.4 pc (2.5-10 arcmin scales at the TMC distance of 140 pc). A fine tuning between resolution and statistics is required. The star counts method is better suited for this purpose.

4.2 Star counts

Since the seminal work by van Rhijn (1929), star counts have been used to measure extinction in galactic fields. A detailed description of the method is given by Bok & Cordwell (1973). This technique has been extensively used in as-

tronomy and has been successfully applied to measure the gas column to Taurus using the R plate of the Palomar Observatory Sky Survey (Cernicharo & Bachiller, 1984).

Basically, the apparent magnitude of a given star in the NUV band, $m(NUV)$, is given by:

$$m(NUV) - M(NUV) = -5 + 5 \log \frac{d}{\text{pc}} + A_{NUV} \quad (15)$$

where $M(NUV)$ is the absolute magnitude, d is the distance and A_{NUV} is the extinction in the NUV band caused by the intervening gas. In its most usual application, star counts in a given field are compared with the predictions for an unextinguished, nearby field and the extinction is given by,

$$A_\lambda = \log(N_\lambda^*/N_\lambda)/b_\lambda \quad (16)$$

where N_λ are the observed counts, N_λ^* are the expected counts from a non-extinguished field, and $b_\lambda = d \log N(m_\lambda)/dm_\lambda$ (with m_λ the apparent magnitude at wavelength λ) is a measure of the slope of the luminosity function in the area under study.

The NUV luminosity function has not been determined for the Galaxy thus we have derived it in this work for the TMC region. Firstly, we have determined it for the reference field (AIS189_28), which we consider unextinguished and has 2,340 sources. We have calculated it to be well fitted by,

$$\log N(m_{NUV}) = (0.294 \pm 0.002)m_{NUV} - 2.55 \pm 0.04$$

with $RMS = 0.046$ and thus, $b_{NUV} = 0.294$ (see Fig. 6). We also have tested whether there are significant variations over the TMC field. As shown in the bottom panel of Fig. 6, the slope remains constant (within the error bars) pointing out that only minor variations are detected over the field, if any.

The accuracy of the A_{NUV} values derived from the star counts method is (see Dickman 1978),

$$\frac{\delta NUV}{NUV} = (\log \frac{N_{NUV}^*}{N_{NUV}})^{-1} (\frac{N_{NUV} + N_{NUV}^*}{N_{NUV} N_{NUV}^*})^{1/2} \quad (17)$$

with,

$$\delta A_{NUV} = \frac{1}{b_{NUV}} (\frac{N_{NUV} + N_{NUV}^*}{N_{NUV} N_{NUV}^*})^{1/2} \quad (18)$$

Thus, for $A_{NUV} = 0$ (or $N_{NUV}^* = N_{NUV}$), $\delta A_{NUV} = 0.1$ mag.

The maximum A_{NUV} is observed in tile AIS190_43 with $N_{NUV} = 136$, and thus $A_{NUV} = 3.2$ mag with $\delta A_{NUV} = 0.3$ mag.

If the statistics are good then both the Wolf and star-counts should produce very similar results. Average A_{NUV} s have been calculated by both methods for all the GALEX fields and, as shown in Fig. 7, the only discrepancy is at high extinctions (low star counts) since the Wolf method produces slightly higher extinctions than the star-counts method. The regression line is:

$$A_{NUV}(\text{Wolf}) = (1.10 \pm 0.03)A_{NUV}(\text{Counts}) + (0.08 \pm 0.04)$$

with $rms = 0.27$.

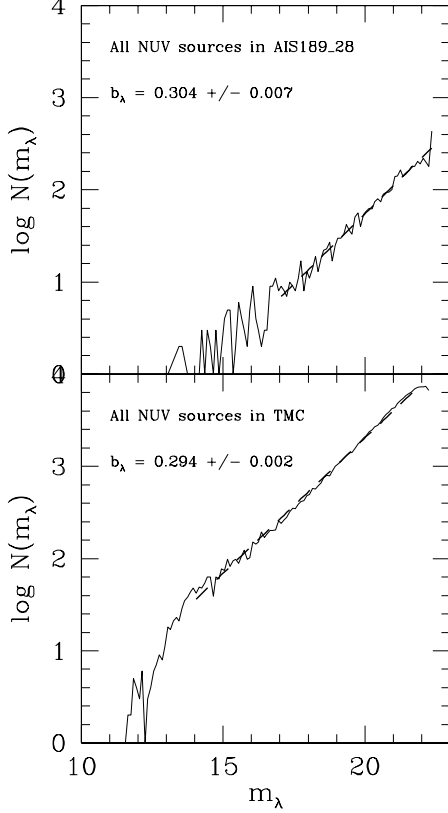


Figure 6. Stellar luminosity function in the TMC in the NUV band. **Top:** NUV luminosity function in the reference field, **bottom:** luminosity function derived from all NUV sources in the AIS TMC survey. The best fit to the slope is shown by a dashed line on the fitted region.

4.3 Galactic latitude correction

Stellar density declines significantly with galactic latitude⁵. To correct for this effect, we have computed the variation of N_{NUV}^* with galactic latitude and derive a correction factor, dA , such that,

$$A_{NUV}^0 = A_{NUV} - dA_{NUV} \quad (19)$$

⁵ As pointed out in the text, we have not found significant variations in the luminosity function, as a simple inspection of Fig. 6 shows.

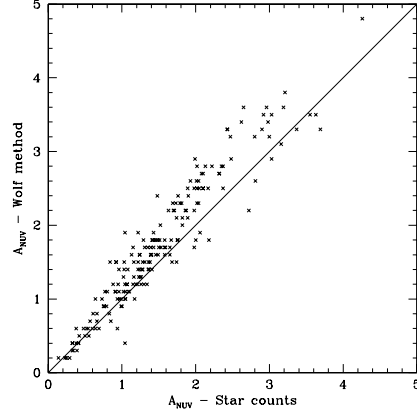


Figure 7. Comparison between the A_{NUV} values obtained by direct star counts and by using the Wolf method. The straightline marking A_{NUV} - Wolf method equal to A_{NUV} - Star counts is plotted for comparison.

being A_{NUV} , the extinction determined with the star counts method, Eq. 16, and A_{NUV}^0 , the final value of extinction. To evaluate this correction, we have made use of the Besancon model of the Galaxy (Robin et al. 2003; Czekaj et al. 2014, see also URL: model.obs-besancon.fr), and the A_K map of the TMC evaluated by LLA10 (see details in Appendix B). The correction factor is found to be,

$$dA = (0.0640 \pm 0.0005)b_{gal}(^{\circ}) - (0.38 \pm 0.01) \quad (20)$$

(with $rms = 0.025$).

The variation of the stellar luminosity function between $l_{gal} = 165^{\circ}$ and $l_{gal} = 180^{\circ}$ is negligible according to the Besancon standard model.

5 RESULTS: VARIATION OF A_{NUV}/A_K OVER THE TMC

Cores and filaments in molecular clouds have typical physical scales of 0.1-0.4 pc that correspond to 2.5-10 arcmin at the TMC distance (140 pc). Unfortunately, the UV statistics is too poor at resolutions of 3 arcmin² (see Fig. 4). Thus, we have followed an incremental approach using two intermediate bin sizes of 24 arcmin² and 12 arcmin².

NUV extinctions have been calculated by applying the star counts method (see Sect. 4) including the galactic latitude correction derived in Appendix B. To compute K-extinctions we have resourced directly to Froebrich et al. (2007) map. The map has been rebinned and re-scaled to K-magnitude; note that F07 provide the electronic version of the map (FITS format) in visual extinctions (A_V), but these A_V values are obtained by the authors after applying a simple scaling from infrared to visual magnitudes assuming that the standard ISM extinction law holds (Draine 1989).

As shown in Fig. 8, there is a significant variation of

A_{NUV}/A_K across the region. $A_{NUV}/A_K \simeq 33$ in the diffuse ISM, around the TMC in agreement with FM07. However, westwards, at the tail of the cloud, where the main filaments reside, and the column density of molecular gas increases, A_{NUV}/A_K decreases pointing out the weakening of the UV bump and, in general, a larger average size of the dust grains when compared with the diffuse ISM. This trend is confirmed at both intermediate resolutions.

Some of the areas mapped by GALEX have very low and thus, uncertain, A_K values (LLA10 estimates $dA_K = \pm 0.04$ mag). This results in abnormally high A_{NUV}/A_K rates, especially at high galactic latitudes (see Fig. 8).

Experimentally, the UV bump is known to be produced by mixtures of sufficiently large, neutral PAHs (Steglich et al. 2011). Moreover, the UV-visible measurements provide a reliable fingerprint of the presence of specific PAHs since the electronic transitions of these species are detected in this range while the near infrared vibrational bands are not molecule specific.

A recent UV-visible (3050-3850 Å) study based on the observations towards five lines of sight with moderate reddenings measured PAHs abundances two orders of magnitude smaller than those in the diffuse ISM (Gredel et al. 2011); the measurements were made over column densities of $N_H = 5.7 - 9.2 \times 10^{21} \text{ cm}^{-2}$, slightly above the dominant column density of our study in the TMC, $N_H \leq 4 \times 10^{21} \text{ atoms cm}^{-2}$. This study was sensitive to molecules such as anthracene, pyrene or benzofluorene. Laboratory experiments suggest that the UV bump is produced by larger PAHs with sizes above 50-60 carbon molecules (Steglich et al., 2010) thus, our results suggests that large PAHs are neither abundant in translucent clouds.

A_{NUV}/A_K is small close to the filamentary networks (compare Fig 3 with Fig 8) where also mid infrared data have detected the formation of large dust grains (Flagey et al. 2010), as high density of molecular gas makes collisional processes more efficient assisting grain growth. In addition, the large density of dust in the filaments effectively shields the growing mantles against the environmental UV radiation. A detailed comparison between Figure 4 and 8, shows that the bump is less prominent towards the tail of the filaments leading to L1495 and L1498. The first results from the Herschel survey of the Gould Belt in Taurus, show a fraction of this area: N1-3 for the filament leading to L1495 and S1-4 for that leading to L1498. The analysis of Herschel data shows that these filaments consist really in a hierarchy of cores of molecular gas with sizes in the range 0.0242.7pc that covers the full core mass function from unbound clumps to (gravitationally bound) pre-stellar cores, being all part of the same population (Kirk et al. 2013). Our detection of increased average size of dust grains around this area is consistent with the enhancement of the molecular gas and dust density that drives the formation of molecular cores.

In the global scenario developed by GdCP92, matter in the TMC is being gathered by the local action of the Parker-Jeans instability. Matter lifted to the halo by the action of the instability, rains back along the magnetic field lines reaching velocities comparable to the Alfvén speed in the undisturbed gas layer in the galactic plane. These velocities agree well with the clouds and pre-main sequence stars velocities that roughly run eastwards (see GdCP92). Fresh material is thus expected to be gathered at the rear

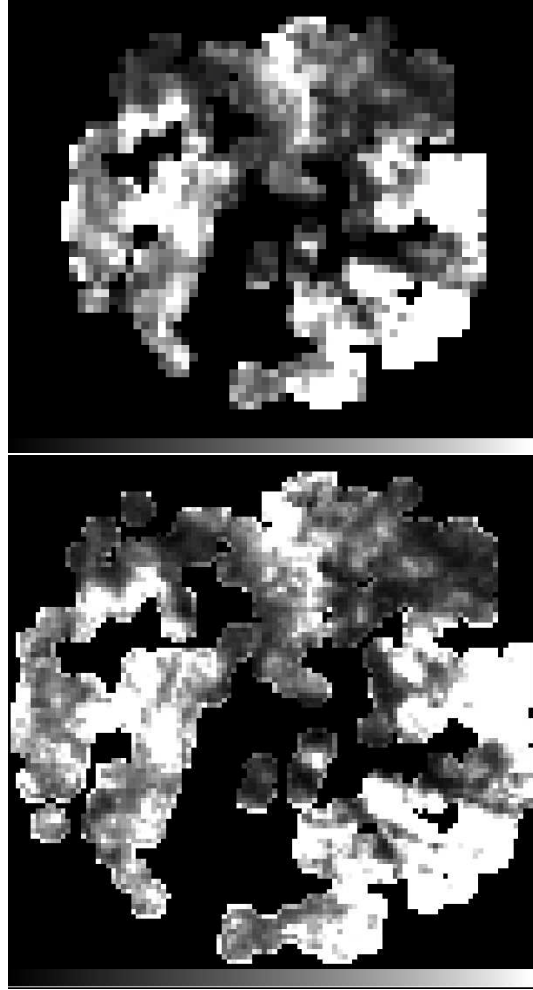


Figure 8. A_{NUV}/A_K on the TMC computed for bins of 24 arcmin² and 12 arcmin², top and bottom panels respectively. The gray scale runs from $A_{NUV}/A_K = 0$ (black) to $A_{NUV}/A_K \geq 33$ (white). $A_{NUV}/A_K \geq 33$ corresponds to the predictions of the standard ISM extinction law (see Table 1).

of the cloud, where it is, indeed. As the density increases with respect to the average ISM values, so does the opacity protecting dust grains from the ambient UV radiation field and favouring grain growth. In this sense, our results are consistent with the expectations. Unfortunately, the long wavelength Alfvén wave mapped by Moneti et al. (1984) was not properly surveyed by GALEX.

6 CONCLUSIONS

In this work, we have shown the potentials of wide field UV imaging to study the distribution and properties of diffuse dust clouds in space. Our main contributions to the analysis of the UV data have been:

- to show that the wide field UV images obtained by means of the GALEX AIS are able to detect very low dust columns that are not detected through infrared surveys (2MASS). These images are obtained with a rather modest telescope (40 cm) in 150 s (barely 2.5 minutes), in average.
- the stars luminosity function has been derived for the

GALEX NUV band in the galactic anticenter region. b_{NUV} has been computed. This value is suitable to be compared with measurements across the Galaxy.

- a generic method to determine the relative abundance of small dust grains from star counts and surveys has been described.

These developments have been used to detect variations in the extinction law across the TMC. The extinction law tends to be greyer in the rear of the cloud and in the networks of filaments, than on the clean ISM. This is consistent with the generic picture of large dust grains being formed in molecular clouds and small dust grains being more abundant in the ISM. It is worth remarking that the areas where dust is being gathered are at the rear of the cloud, as expected if star formation at the head of the TMC is associated with a local storage of mass being gathered by the action of the Parker-Jeans instability.

Unfortunately, the depth of the GALEX AIS is not enough to have good statistics in the areas around the filaments so, we cannot test effects like grain growth. Note that according to,

$$A_{NUV}^{lim} \simeq \log(N_{NUV}^*/N_{NUV}^{lim})/0.29$$

and setting $N_{NUV}^{lim} = 1$, A_{NUV}^{lim} depends on the number of sources in the test field (which is the maximum) and thus, on the resolution. To reach spatial resolutions of 0.05 pc, reasonable to study the filaments structure, and $A_{NUV}^{lim} = 4$, it is required that $N_{NUV}^* = 16$ per 1.2 arcmin², which represents a factor of 14 increase in stellar density (stars/arcmin²) with respect to GALEX AIS. The limiting magnitude should rise from $NUV = 22.3$ mag (see Gómez de Castro et al. 2015) to $NUV = 23.5$ mag.

ACKNOWLEDGMENTS

This work has been partially funded by the Ministry of Science and Innovation of Spain through grant: AYA2011–29754-C03-C01 and AYA2011–29754-C03-C03. This article is based on data obtained by the NASA mission Galactic Evolution Explorer (GALEX).

REFERENCES

Arce, H.G., Goodman, A. A., 1999, ApJ, 517, 264
 Benson, P. , Myers, P.C., 1983, ApJ , 270, 589
 Bianchi, L., 2014, Ap&SS, 354, 103
 Bok, B.J., Cordwell, C.S., 1973, Molecules in the Galactic Environment, Proceedings of a Symposium, held at the University of Virginia, November 4-7, 1971, Edited by M.A. Gordon, and Lewis E. Snyder. New York, NY: John Wiley and Sons, p.54
 Cernicharo, J., Bachiller, R., 1984 A&AS , 58, 327
 Cutri, R.M., Wright, E.L., Conrow, T. et al., 2012, Explanatory Supplement to the WISE All-Sky Data Release Products
 Czekaj, M.A., Robin, A.C., Figueras, F. et al., 2014, A&A, 564, 102
 Chapman, N.L., Goldsmith, P.F., Pineda, J.L. et al., 2011, ApJ , 741, 21

Davis, C.J., Chrysostomou, A., Hatchell, J., et al, 2010, MNRAS , 405, 759
 Dickman, R.L., 1978, AJ, 83, 363
 Draine, B.T., Malhotra, S., 1993, ApJ, 414, 632
 Draine, B.T., 1989, Interstellar Dust: Proceedings of the 135th Symposium of the International Astronomical Union, held in Santa Clara, California, 26-30 July 1988. Edited by Louis J. Allamandola and A. G. G. M. Tielens. International Astronomical Union. Symposium no. 135, Kluwer Academic Publishers, Dordrecht, p.313
 Draine, B.T., 2003, ARA&A, 41, 241
 Dunham, M., Stutz, A., Allen, L. et al. 2013, Protostars and Planets VI, in press.
 Elmegreen, B. G., 1990, ApJ, 357, 125
 Fitzpatrick, E.L., Massa, D., 2007, ApJ, 663, 320 (FM07)
 Flagey, N., Noriega-Crespo, A., Boulanger, F., et al. 2009, ApJ, 701, 1450
 Franco, J., Kim, J., Alfaro, E.J. et al. , 2002, ApJ , 570, 647
 Froebrich, D., Murphy, G. C., Smith, M. D., Walsh, J., & Del Burgo, C. 2007, MNRAS, 378, 1447 (F07)
 Gaida, M., Ungerechts, H., Winnewisser, G., 1984, A&Ap, 1387, 17
 Goldsmith, P.F., Heyer, M., Narayanan, G., et al. 2008 , ApJ , 680, 428
 Goldsmith, P.F., Velusamy, T., Li, D. et al., 2010, ApJ, 715, 1370
 Gómez de Castro, A.I., and Pudritz, R.E., 1992, ApJ, 395, 501
 Gómez de Castro, A.I., López-Santiago, J., Sestito, P. et al. 2011, ApSS, 335, 97
 Gómez de Castro, A.I., López-Santiago, J., López-Martínez, F. et al. 2015, ApJS, 216, 26
 Goodman, A.A., Bastien, P., Menard, P. et al., 1990, ApJ , 359, 363
 Goodman, A.A., Pineda, J.E., Schnee, S.L., 2009, ApJ , 692, 91
 Gorbikov, E., Brosch, N., 2010, MNRAS, 401, 231
 Gredel, R., Carpentier, Y., Rouillé, G., et al., 2011, A&A, 350, 26
 Haywood, M., Robin, A.C., Creza, M., 1997, A&A, 320, 428
 Heyer, M.H., Vrba, F.J., Snell, R.L. et al., 1987, ApJ, 321, 855
 Heyer, M.H., Brunt, C.M., 2012, MNRAS , 420, 1562
 Kirk, J.M., Ward-Thompson, D., Palmeirim, P., et al., 2013, MNRAS, 432, 1424
 Kuijken, K., Gilmore, G., 1989, MNRAS, 239, 651
 Lada, E., 1992, ApJ, 393, L25
 Ladd, E. F., Myers, P. C., Goodman, A. A., 1994, ApJ, 433, 117
 Lee, D.-H., Yuk, I.-S., Jin, K., et al. 2006, ApJ 644, L181
 Leger, A., Puget, J.L., 1984, A&A, 137, L5
 Lombardi, N., 2009, A&A, 493, 735
 Lombardi, N., Lada, C.J., Alves, J., 2010, A&Ap , 512, 67
 Mirabel, I. F. 1982, ApJ, 256, 112
 Moneti, A., Pipher, J.L., Helfer, H.L. et al., 1984, ApJ , 282, 508
 Morrissey, P., Conrow, T., Barlow, T. A., et al. 2007, ApJ, 173, 697
 Myers, P.C., Benson, P.J., 1983, ApJ, 266, 309
 Nakano, T., 1998, ApJ, 494, 494, 587

- Ojha, D.K. 2001, MNRAS, 322, 426
 Olano, C.A., Walmsley, C.M., Tisley, T.L., 1988, A&Ap , 196, 1940
 Pilipp, W., Morfill, G.E., Harquist, T.W. et al., 1987, ApJ , 314, 341
 Robin, A. C., Reyle, C., Derriere, S., et al. 2003, A&A, 409, 523
 Siess, L., Dufour, E., Forestini, M., 2000, A&A, 358, 593
 Steglich, M., Jger, CX., Rouillé, G., et al. 2010, ApJ, 712, L16
 Steglich, M., Bouwman, J., Huysen, F., 2011, ApJ, 742, 2
 Strutskie, M.F., Cutri, R.M., Stiening, R., et al. 2006, AJ, 131, 1163
 Ungerechts, H., Thaddeus, P., 1987, ApJSS, 63, 645
 Vrba, F.J., Strom, S.E., Strom, K.M., AJ , 81, 958
 van Rhijn, P.J., 1929, Publications of the Kapteyn Astronomical Laboratory Groningen, 43, 1
 Wada, S., Kaito, C., Kimura, S. et al. 1999, A&A, 345, 259
 Wang, J.-J., Chen, W.-P., Miller, M. et al, ApJ, 614 L105
 Weingartner, J.C., Draine, B.T., 2001, ApJ, 553, 581
 Wolf, M. 1923, Astronomische Nachrichten 219, 109
 Ysard, N., Abergel, A., Ristorcelli, I., et al. 2013, A&A , 559, 133
 Yuan, H.B., Liu, X.W., Xiang, M.S., 2013, MNRAS, 430, 2188
 Zacharias, N., Finch, C. T., Girard, T. M., et al. 2013, AJ, 145, 44

APPENDIX A: ESTIMATE OF THE IMPACT ON THE A_{NUV}/A_K RATE OF THE FILLING FACTOR OF THE DUST CLOUDS WITHIN THE GALEX AIS FIELD OF VIEW

Let A_{NUV} and A_K be the extinctions evaluated from the star counts and affected by the filling factor of the extincted over un-extincted areas in the field of view. Let A_{NUV}^f and A_K^f the true, average values, taking into account only the extincted areas. Then,

$$\log \frac{N_{NUV,max}}{N_{NUV}} = b_{NUV} A_{NUV}^f \quad (A1)$$

$$\log \frac{N_{K,max}}{N_K} = b_K A_K^f \quad (A2)$$

and,

$$\delta A_{NUV} = \frac{1}{b_{NUV}} \log \chi = A_{NUV}^f - A_{NUV} \quad (A3)$$

$$\delta A_K = \frac{1}{b_K} \log \chi = A_K^f - A_K \quad (A4)$$

with δA_{NUV} and δA_K the excess extinctions caused by the geometric filling factor of dusty areas in the GALEX field of view, χ . With this definition,

$$\frac{A_{NUV}}{A_K} = \frac{b_K}{b_{NUV}} \frac{b_{NUV} A_{NUV}^f - \log \chi}{b_K A_K^f - \log \chi} \quad (A5)$$

and after some algebra,

$$\frac{1}{b_{NUV}} \log \chi = A_{NUV}^f \frac{\frac{A_{NUV}}{A_K} \frac{A_K^f}{A_{NUV}^f} - 1}{\frac{b_{NUV}}{b_K} \frac{A_{NUV}}{A_K} - 1} \quad (A6)$$

$$\frac{1}{b_K} \log \chi = A_K^f \frac{\frac{A_{NUV}}{A_K} - \frac{A_{NUV}^f}{A_K^f}}{\frac{A_{NUV}}{A_K} - \frac{b_K}{b_{NUV}}} \quad (A7)$$

or,

$$\delta A_{NUV} = A_{NUV}^f \frac{\frac{A_{NUV}}{A_K} \frac{A_K^f}{A_{NUV}^f} - 1}{\frac{b_{NUV}}{b_K} \frac{A_{NUV}}{A_K} - 1} \quad (A8)$$

$$\delta A_K = A_K^f \frac{\frac{A_{NUV}}{A_K} - \frac{A_{NUV}^f}{A_K^f}}{\frac{A_{NUV}}{A_K} - \frac{b_K}{b_{NUV}}} \quad (A9)$$

making use of the b_K and b_{NUV} values determined from the luminosity functions (see Sect. 4.1) and assuming $A_{NUV}^f/A_K^f = 33.01$, the average ISM value, we derive,

$$\frac{\delta A_{NUV}}{A_{NUV}^f} = \frac{\frac{A_{NUV}}{A_K} \frac{1}{33.01} - 1}{0.94 \frac{A_{NUV}}{A_K} - 1} \quad (A10)$$

$$\frac{\delta A_K}{A_K^f} = \frac{\frac{A_{NUV}}{A_K} - 33.01}{\frac{A_{NUV}}{A_K} - 1.07} \quad (A11)$$

Finally, note that $(A_{NUV} - A_K)$ is basically insensitive to the filling factor since,

$$A_{NUV} - A_K = \frac{1}{b_{NUV}} \log \frac{N_{NUV,max}}{N_{NUV}} - \frac{1}{b_{NUV}} \log \chi \quad (A12)$$

$$A_{NUV} - A_K = \frac{1}{b_K} \log \frac{N_{K,max}}{N_K} - \frac{1}{b_K} \log \chi \quad (A13)$$

$$A_{NUV} - A_K = A_{NUV}^f - A_K^f - \left(\frac{1}{b_{NUV}} - \frac{1}{b_K} \right) \log \chi \quad (A14)$$

assuming $b_{NUV} \simeq b_K$. Unfortunately, this colour has a softer dependence on the strength of the 2175 Å bump than the rate A_{NUV}/A_K as shown in Sect. 2.

This short exercise provides a first order estimate and neglects the effects caused by the cloud clumpiness (see, for instance, Lombardi 2009).

APPENDIX B: DERIVATION OF THE CORRECTION FOR GALACTIC LATITUDE

The GALEX AIS survey spans over a wide range of galactic latitudes (from $b_{gal} \simeq -5^\circ$ to $b_{gal} \simeq -25^\circ$) and it is expected that the stellar density decreases significantly over the surveyed area. As a result, in the evaluation of the extinction:

$$A_\lambda = \log(N_\lambda^*/N_\lambda)/b_\lambda$$

N_λ^* is a function of b_{gal} . In our work, we have used only a reference field, AIS189-28, located at $b_{gal} = -6^\circ$ hence it is necessary to determine the correction term, δA_{lambda} , such that,

$$dA_\lambda(b_{gal}) = \frac{1}{b_{lambda}} \log \left(\frac{N^*(-6^\circ)}{N(b_{gal})} \right)$$

To derive it, we have used the infrared data and a simplified model of the galactic stellar density distribution.

LLA10 reported that the K-band star counts followed the galactic model. Both FM07 and Lombardi et al (2010) designed procedures to correct for this gradient so they provide a reliable baseline to compare our correction with. Note

that no significant variations are expected in b_λ . Neither the stellar density varies significantly with galactic longitude in the anticenter region.

The impact of this correction in extinction determinations is illustrated in Fig. B1. Rough A_K (without δA_K correction) have been computed by applying the star counts method on the sample constituted by **all bona fide** 2MASS sources in any given of the GALEX fields to the depth of the 2MASS survey (see Fig. B1, top panel), as well as to a reduced sample including only the 2MASS sources with NUV counterpart. Both panels display a clear gradient with galactic latitude, more pronounced in the top panel. At the bottom, F07's infrared extinction map is shown for comparison (the map has been rebinned to the GALEX tiles size and distribution).

According to the standard galactic model, the stellar density, ρ^* , in the Galaxy can be parametrized in terms of a thin, ρ_a^* , and a thick disk, ρ_b^* , as follows:

$$\rho^* = \rho_a^* + \rho_b^* \quad (\text{B1})$$

with,

$$\rho_{a,b}^* = \rho_{0,(a,b)}^* \exp\left(-\frac{R}{L_{a,b}}\right) \exp\left(-\frac{z}{H_{a,b}}\right) \quad (\text{B2})$$

with, R and z the galactocentric cylindric coordinates in the disk (cylindric symmetry is assumed) and $\rho_{0,a}^*$ and $\rho_{0,b}^*$ the volumetric density of stars in the center of the thin and thick disk, respectively. According to Ojha (2001), the parameters for the model are: $L_a = 2.8 \pm 0.3$ kpc, $L_b = 3.7^{+0.8}_{-0.5}$ kpc, $H_a = 250$ pc (Kuijken & Gilmore 1989, Haywood 1997), $H_b = 860 \pm 200$ pc and $\rho_{0,b}^*/\rho_{0,a}^* = 0.035 \pm 0.02$. With these provisions, the total number of stars with absolute magnitude, M , observed within a solid angle, Ω , up to a given depth r_d , is given by,

$$N(M) = \int_0^{r_d} \Phi(M) \rho^* \Omega r^2 dr \quad (\text{B3})$$

with $\Phi(M)$ the galactic distribution of stars with absolute magnitude, M . Let us assume that $\Phi(M)$ can be consider constant and equal to Φ_0 for all the sources in our survey. This would imply that all sources follow the simple parametrization in Eq. (B2), irrespective of their nature, on scales of 1.4 deg (the resolution of the survey). With this approach,

$$N(r_d) = \Phi_0 \int_0^{r_d} \rho^* \Omega r^2 dr \quad (\text{B4})$$

Since the galactic longitude of our region of interest is $l_{gal} \simeq 180^\circ$, $z \simeq (r + r_\odot) \tan(b_{gal})$, with r_\odot the galactocentric distance of the Local Standard of Rest (LSR) and (r, l_{gal}, b_{gal}) the LSR-centric galactic coordinates. Then,

$$\frac{dN(r_d)}{\cos b_{gal} db_{gal} dl_{gal}} = \quad (\text{B5})$$

$$\begin{aligned} & \Phi_0 \left(\exp\left(-\frac{r_\odot}{L_a}\right) \int_0^{r_d} \exp\left(-r\left(\frac{1}{L_a} + \frac{\tan b_{gal}}{H_a}\right)\right) r^2 dr \right. \\ & \left. + 0.035 \exp\left(-\frac{r_\odot}{L_b}\right) \int_0^{r_d} \exp\left(-r\left(\frac{1}{L_b} + \frac{\tan b_{gal}}{H_b}\right)\right) r^2 dr \right) \end{aligned} \quad (\text{B6})$$

Lets denote,

$$S_{a,b} = \frac{1}{L_{a,b}} + \frac{\tan b_{gal}}{H_{a,b}} \quad (\text{B7})$$

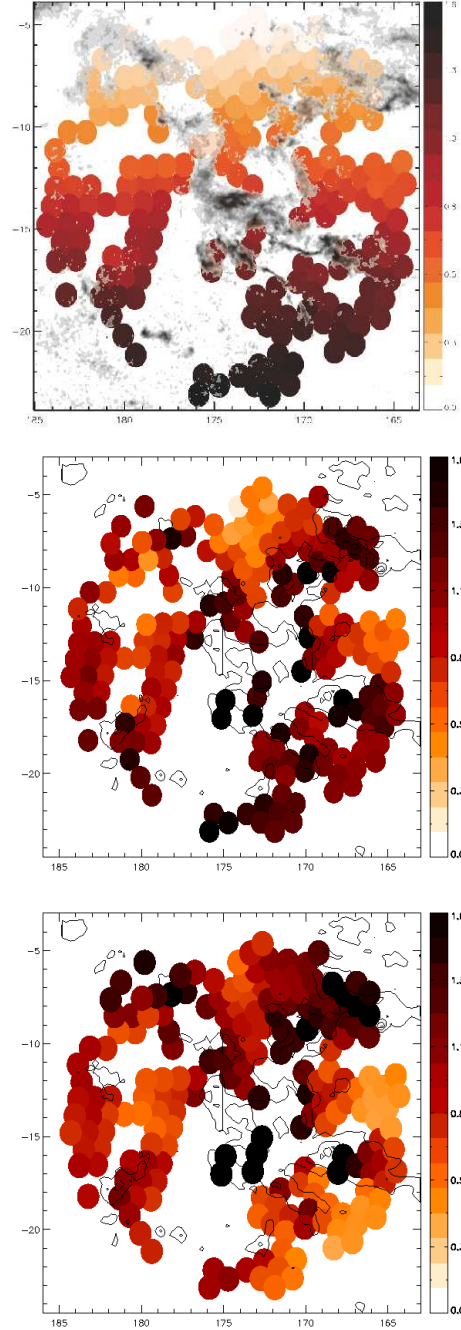


Figure B1. K-band color-coded average extinction per GALEX AIS tile in the TMC. *Top:* δA_K derived from all 2MASS sources per GALEX tile, *Middle:* δA_K derived from stars with NUV counterpart, *Bottom:* δA_K derived from binning F07 2MASS based extinction map.

Then,

$$\begin{aligned} & \frac{dN(r_d)}{\cos b_{gal} db_{gal} dl_{gal}} = \Phi_0 \times \\ & \left(\exp\left(-\frac{r_\odot}{L_a}\right) \int_0^{r_d} \exp(-r S_a) r^2 dr \right. \end{aligned} \quad (\text{B8})$$

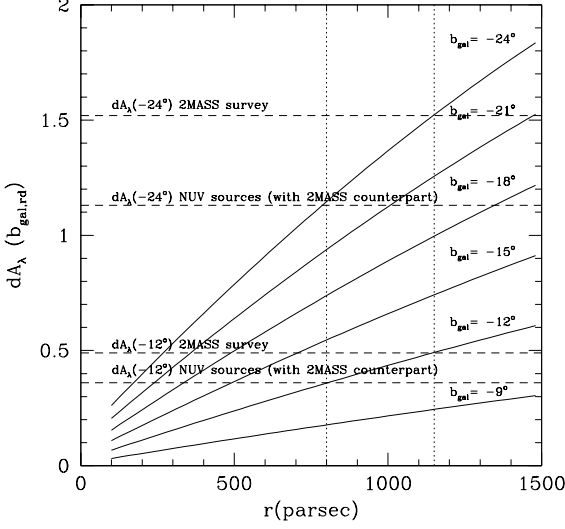


Figure B2. Effect of the variation of stellar density with galactic latitude in the extinctions computed from star counts with a given reference field at $b_{gal} = -6^\circ$

$$+0.035 \exp(-r_\odot/L_b) \int_0^{r_d} \exp(-rS_b) r^2 dr$$

that depends on galactic latitude and depth of the survey. Let us denote,

$$n(b_{gal}, r_d) = \frac{dN(r_d)}{db_{gal} dl_{gal}} \quad (\text{B9})$$

and,

$$dA_\lambda(b_{gal}, r_d) = \frac{1}{b_{lambda}} \log \left(\frac{n^*(-6^\circ, r_d)}{n(b_{gal}, r_d)} \right) \quad (\text{B10})$$

the effect of the stellar density gradient in the extinction derived from star counts. Note that Eq.(B10) is parametrized in terms of the reference field AIS189.28 (see Sect. 5), at $b_{gal} = -6^\circ$.

In Fig. B2, $dA_\lambda(b_{gal}, r_d)$ is plotted for a range of galactic latitudes and possible depths of the surveys according to Eq. (B10). To determine the depth of the survey (and the proper correction to be applied), we have used three tiles, at different galactic latitudes: the reference tile AIS189.28 ($b_{gal} \simeq -6^\circ$), AIS190.42 ($b_{gal} \simeq -12^\circ$) and AIS169.28 ($b_{gal} \simeq -24^\circ$). We have cross-checked that $A_K = 0$ for all of them in the LLA10 extinction map.

We have used A_K measurements (see Fig. B1) to evaluate $dA_\lambda(-12^\circ, r_d) = A_\lambda(\text{AIS190.42}) - A_\lambda(\text{AIS189.28})$ and $dA_\lambda(-24^\circ, r_d) = A_\lambda(\text{AIS169.28}) - A_\lambda(\text{AIS189.28})$. They are represented by dashed lines in Fig. B2 as, $dA_\lambda(-24^\circ)$ and $dA_\lambda(-12^\circ)$.

As it is noticeable, the dashed lines meet the galactic model at $r_d \simeq 800$ pc, for both galactic latitudes. Thus, we assume that this is the depth of the GALEX AIS survey in this area of the Galaxy. From that, we compute the correction factor to be applied to the measurements in Table 2 to be,

$$dA = (0.0640 \pm 0.0005) |b_{gal} (^\circ)| - (0.39 \pm 0.01) \quad (\text{B11})$$

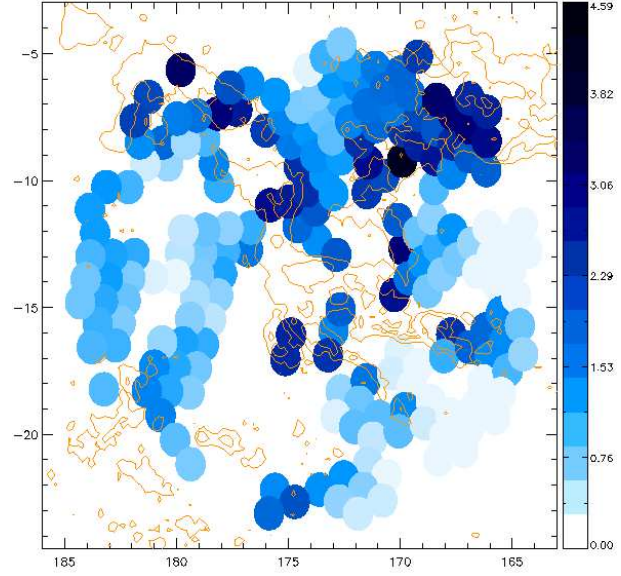
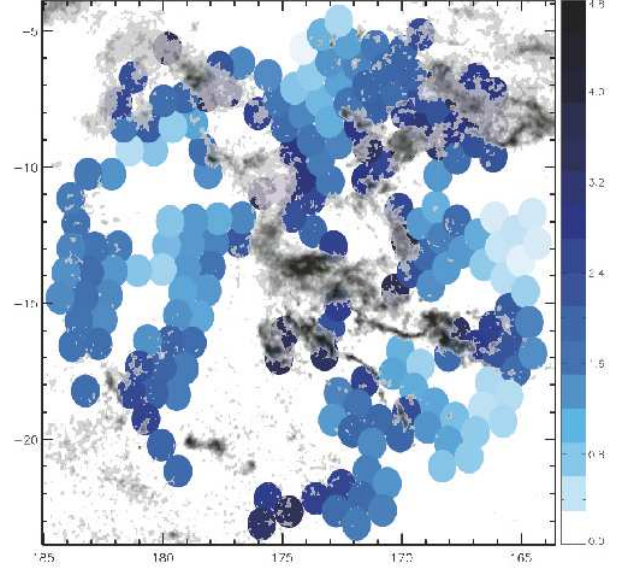


Figure B3. Average extinction per GALEX tile in the NUV band determined from star counts. *Top:* A_{NUV} without applying the δA_{NUV} correction, *bottom:* A_{NUV} after applying the correction. The location of the obscuring clouds from F07 is outlined. Coordinates as in Fig 1.

(with $rms = 0.025$). The extinction map in the NUV band, after applying this correction, is displayed in Fig. B3, for the record. The location of the obscuring clouds, the high latitude cirrus and the filaments are readily shown.

